optica

Nonlinear photonic crystals: from 2D to 3D

Yong Zhang,[1] Yan Sheng,[2,5] Shining Zhu,[1] Min Xiao,[1,3,6] and Wieslaw Krolikowski[2,4]

[1]National Laboratory of Solid State Microstructures, College of Engineering and Applied Sciences, School of Physics, and Collaborative Innovation Center of Advanced Microstructures, Nanjing University, Nanjing, China
[2]Laser Physics Center, Research School of Physics, Australian National University, Canberra, ACT 2601, Australia
[3]Department of Physics, University of Arkansas, Fayetteville, Arkansas 72701, USA
[4]Science Program, Texas A&M University at Qatar, Doha, Qatar
[5]e-mail: yan.sheng@anu.edu.au
[6]e-mail: mxiao@uark.edu

Received 2 December 2020; revised 18 January 2021; accepted 24 January 2021 (Doc. ID 416619); published 12 March 2021

Nonlinear photonic crystals are microstructures with quadratic nonlinearity ($\chi^{(2)}$) that have been extensively used for the generation and control of coherent light at new frequencies. Thanks to the recent invention of 3D $\chi^{(2)}$-nonlinearity engineering techniques using femtosecond laser pulses, studies of intense light interaction with 3D nonlinear photonic crystals are now experimentally feasible. Here we review the latest research advances in nonlinear photonic crystals, focusing especially on the fabrication, characterization, and application of 3D structures. We also discuss the future development of 3D nonlinear photonic crystals with properties and functionalities that are either difficult or virtually impossible to achieve with lower dimensional structures.

https://doi.org/10.1364/OPTICA.416619

1. INTRODUCTION

The process of second-harmonic generation (SHG), in which the strong pump beam excites nonlinear response of the dipoles in the medium (nonlinear polarization) that acts as a source of new wave at doubled frequency, constitutes one of the most fundamental nonlinear optical effects. In fact, its first experimental demonstration in 1961 by Franken *et al*. [1] is now commonly considered as the birth of experimental nonlinear optics. From its inception, this and other parametric frequency conversion processes have continuously been a subject of intensive research efforts. This interest is driven by many already existing and potential applications that rely on the capability of frequency conversions to provide high quality, purity, and stability in light sources at new frequencies. They are being used in a variety of applications ranging from laser pointers, high-energy laser sources, laser material processing, standard and nonlinear optical microscopies [2], and optical signal processing [3] to quantum communication, quantum sensing, and quantum computing [4]. Various frequency conversion processes, including sum and difference frequency generations, have been demonstrated in optical materials with second-order ($\chi^{(2)}$) nonlinearity, including ferroelectric crystals [5] and semiconductors [6,7], as well as certain isotropic media such as glass, where the material's symmetry was broken by using, for example, a DC electric field [8].

As Armstrong *et al*. pointed out in their influential 1962 paper [9], the efficiency of the frequency conversion process depends critically on the so-called phase mismatch, i.e., the difference between the phase velocities of the nonlinear polarization and that of generated optical wave(s). In the case of SHG, the phase mismatch ($\Delta\vec{k}$) is represented by a simple relation between wave vectors of the fundamental ($\vec{k}_1$) and second-harmonic ($\vec{k}_2$) beams: $\vec{k}_2 - 2\vec{k}_1 = \Delta\vec{k}$. The electromagnetic energy oscillates between interacting waves if these phase velocities differ, i.e., $\Delta\vec{k} \neq 0$. The period of these oscillations, known as the coherence length l_c, is governed by the dispersion of the medium such that $l_c = \pi/|\Delta\vec{k}| = \lambda_0/[2(n_{2\omega} - n_\omega)]$, where λ_0 is the fundamental wavelength in vacuum and n_ω, $n_{2\omega}$ are refractive indices of the fundamental and second-harmonic waves, respectively. When the phase velocity of nonlinear polarization and the second-harmonic beam coincide, i.e., when the process is phase-matched ($\Delta\vec{k} = 0$), the electromagnetic energy flows monotonically from the pump to the generated wave. Because of natural optical dispersion of homogeneous nonlinear crystals, $\Delta\vec{k}$ is never zero for waves of the same polarization.

In their fundamental work, Armstrong *et al*. proposed a few methods to overcome the dispersion hurdle so that the phase-matching condition could be fulfilled [9]. For instance, the so-called birefringence phase matching involves interaction of waves with orthogonal polarizations and taking advantage of optical anisotropy of the medium to ensure fulfillment of the phase-matching condition.

Another approach, which is applicable to anisotropic as well as isotropic media, is based on the periodic modulation of the sign of quadratic nonlinearity $\chi^{(2)}$. In fact, this idea constitutes the concept of the so-called quasi-phase matching (QPM). Here the spatial modulation of quadratic nonlinearity, or nonlinearity grating with periodicity Λ, gives rise to reciprocal wave vectors $\vec{G}_m$ (quasi momentum), which represent Fourier components

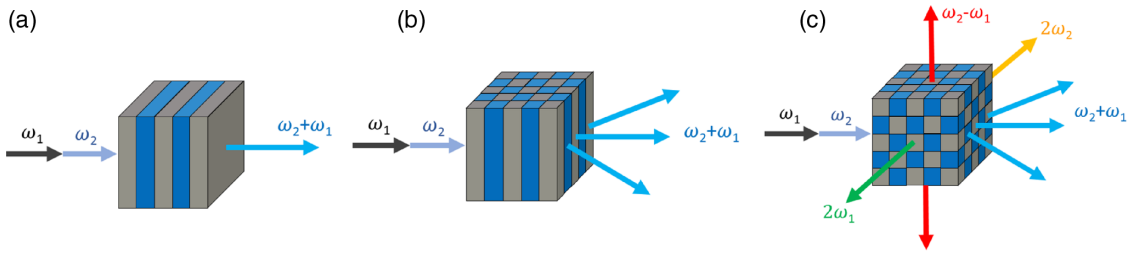

Fig. 1. Schematic illustrations of (a) 1D, (b) 2D, and (c) 3D NPCs, focusing on one of the advantages for 3D configuration, i.e., enabling multichannels of parametric processes with various spatial and spectral resonances.

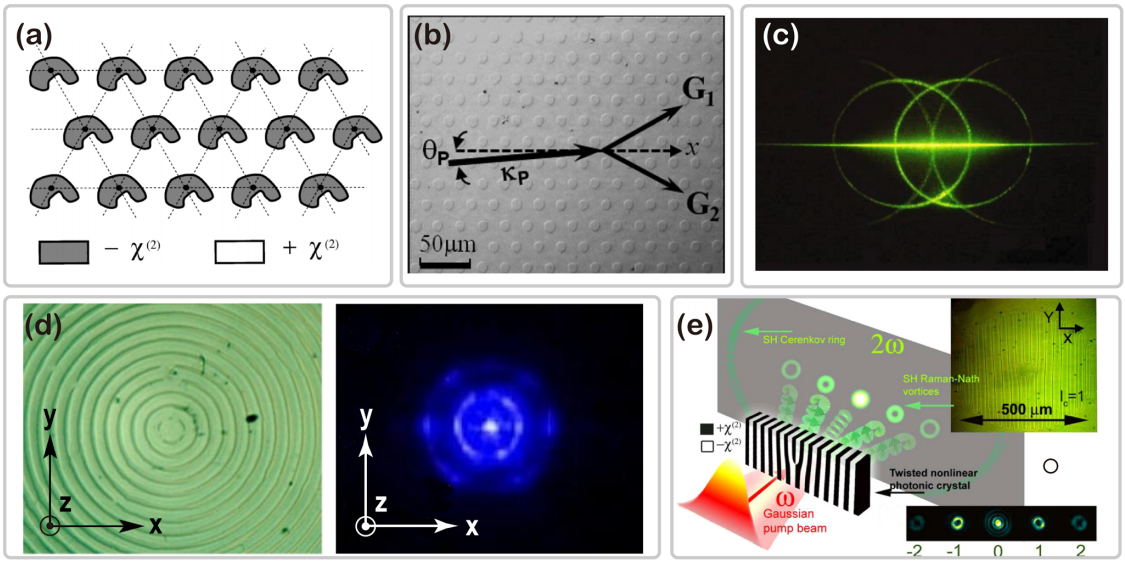

Fig. 2. Several typical experiments in 2D NPCs. (a) Conceptual structure of a 2D NPC [13]; (b) phase-matching configuration in a hexagonally-poled NPC [19]; (c) and (d) present conical SHG via scattering of fundamental beam and nonlinear Raman–Nath diffraction from hexagonal and ring-shaped domain structures, respectively [21,22]; (e) SH vortex beam from a 2D $\chi^{(2)}$-modulated structure [24]. Reproduced from [13,19,21,22,24] with permission.

Table 1. Comparison of Laser-Induced $\chi^{(2)}$ Erasure and $\chi^{(2)}$ Inversion Approaches

	Laser Parameters			
	Pulse Energy	Repetition Frequency	Conversion Efficiency	Applicable Materials
$\chi^{(2)}$ erasure	~100–200 nJ	1 kHz	η	ferroelectric crystals, optical isotropic materials
$\chi^{(2)}$ inversion	~3 nJ	76 MHz	4η	ferroelectric crystals

of the nonlinearity variation and $G_m = 2m\pi/\Lambda$, with m being an integer. The reciprocal vectors contribute to the wave interaction and consequently modify the phase-matching relation. In the case of SHG, the new phase-matching condition now reads: $\vec{k}_2 - 2\vec{k}_1 - \vec{G}_m = 0$. As this relation shows, the phase matching can now be fulfilled by incorporating periodicity of the nonlinearity of the medium. The introduction of such a QPM technique, with its easy implementation in ferroelectric crystals [10–12], has made an enormous impact on the advancement of the research in this field.

Starting from the simplest case of 1D $\chi^{(2)}$ grating, Berger, in his seminal paper, introduced the entirely novel concept of the nonlinear photonic crystal (NPC) (Fig. 1) [13]. In analogy with its linear counterpart, whose spatial refractive index modulations control the ways the light propagates and behaves [14,15], the NPC features spatial periodic modulation of quadratic $\chi^{(2)}$ nonlinearity, maintaining a constant refractive index. While the photonic crystal determines linear light propagation, the NPC controls the properties of nonlinear optical interaction. In particular, by making use of QPM, the NPC introduces spatial and spectral resonances into nonlinear interactions, so efficient emissions of new frequencies can take place along particular spatial directions and only for specific wavelengths. In this context, the simplest nonlinearity grating is just 1D NPC. Going over to nonlinear structures in 2D [Fig. 2(a)], the nonlinear frequency emission conditions are determined not only by basic symmetry of the structure, but also through additional channels involving higher-order QPM processes [Fig. 2(b)] [16–19]. Another, even more relevant, significance of the NPCs lies in their ability to shape the wavefronts of generated waves. To this end, the structure of NPC involves spatially variant nonlinearity distribution, which controls the amplitude shapes of generated waves at new frequencies [Figs. 2(c)–2(e)] [20–24]. This property is important in nonlinear spatial modulation, nonlinear microscopy, and optical tweezers. It has been shown recently that the NPC can play an important role in controlling quantum aspects of frequency conversion. For

instance, the NPCs may allow fabrication of efficient sources of entangled photons in parametric downconversion with spatially engineered characteristics [25,26].

When originally introduced by Berger in 1998, the exploration of NPC was restricted to one and two spatial dimensions because at that time there was no known technique that could be used to modulate $\chi^{(2)}$ nonlinearity in three spatial dimensions. On the other hand, it has been well appreciated that going over to 3D would enormously expand the capabilities of NPCs [13,27–29]. It would, in fact, allow one to create a nonlinear photonic chip in which, by varying the angles and directions of incident waves, one could control the strength and type of nonlinear interaction. Furthermore, the 3D NPCs could enable the realization of true 3D nonlinear volume devices that combine efficient frequency conversion with spatial sculpturing of generated waves in three dimensions (see Fig. 1 for an example).

After almost three decades of intense efforts devoted to nonlinearity controls in quadratic media, two distinct breakthrough techniques, offering actual 3D nonlinearity engineering, have been recently developed [30,31]. They both employ material processing with ultrafast light pulses. In the first approach, the focused pulsed laser beam causes partial destruction of crystalline structure of the material in the focal region, effectively lowering the strength of quadratic nonlinearity in the local areas [30]. The second approach uses tightly focused femtosecond pulses with the peak power below the damage threshold to locally invert spontaneous polarization of the ferroelectric medium. This leads to the formation of local, micrometer-size ferroelectric domains with the sign of the second-order nonlinearity $\chi^{(2)}$ reversed as compared to that of the surrounding crystal [31]. By using either approach, one can scan the nonlinear medium in any spatial locations, efficiently creating desired 3D $\chi^{(2)}$ nonlinearity patterns, which constitute the elusive 3D NPCs [32].

In addition to the unique capability for 3D engineering of optical nonlinearity, ultrafast laser writing is also a promising fabrication technique for linear photonic devices, owing to its versatility to directly create complex structures such as refractive-index gratings, waveguides, and optical microcavities with fine precision [33–35]. The direct laser writing technique has been employed in a wide range of materials, including crystals, glasses, and polymers for various applications. The recent extension of the technique to various ferroelectric crystals paves the way to achieve monolithic fabrication of 3D nonlinear integrated photonic devices for all-optical communication and on-chip signal processing.

In this mini-review, we will first go over the recent advances in fabricating NPCs with the above mentioned femtosecond laser methods, then discuss the characterization techniques for 3D NPCs, and finally give several examples of unique applications of 3D $\chi^{(2)}$ structures in the generation and control of coherent light waves at new frequencies. At the end we discuss some new potential research directions which may benefit from these newly generated 3D NPCs.

2. ALL-OPTICAL FABRICATIONS OF NPCs

A. Laser $\chi^{(2)}$ Erasing Approach

By using a focused femtosecond laser beam to selectively erase $\chi^{(2)}$, a 3D $LiNbO_3$ NPC was first experimentally realized by Wei *et al*. in 2018 [30]. Figure 3(a) shows a microscopic image of the obtained 3D structure. The aim of such laser erasing technique is

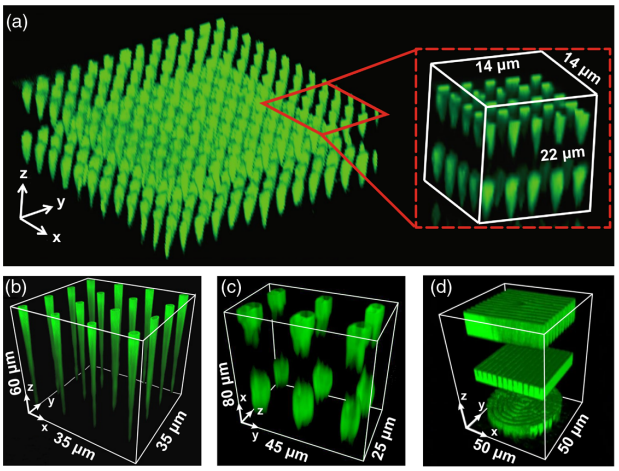

Fig. 3. Nonlinear microscopic images of (a) 3D NPCs fabricated in a $LiNbO_3$ crystal by femtosecond laser erasing of the second-order nonlinearity $\chi^{(2)}$ [30] and (b)–(d) 2D and 3D NPCs fabricated by domain inversion in $LiNbO_3$ [43], $Ba_{0.77}Ca_{0.23}TiO_3$ [31], and $Ca_{0.28}Ba_{0.72}Nb_2O_6$ crystals [46], respectively. These images are obtained using the Čerenkov SH microscopy. Reproduced from [30,31,43,46] with permission.

quite different from the traditional NPC fabrication techniques. Instead of trying to invert ferroelectric domains, the laser parameters are optimized to selectively erase the nonlinear coefficient(s) of the $LiNbO_3$ crystal. The strong light–matter interaction will lower the crystallinity of the $LiNbO_3$ crystal and therefore erase or reduce $\chi^{(2)}$ locally. As shown in [30], the local second-harmonic (SH) signal from the central laser-erased area can be suppressed to as low as ~20% of its original value.

With the $\chi^{(2)}$-erasing method, 3D $LiNbO_3$ NPCs that are capable of nonlinear beam shaping were also fabricated [36,37]. The light source used was a mode-locked Ti:Sapphire femtosecond laser system with a regenerative amplifier (such as Legend Elite-1K-HE Coherent). Typically, the pulse width is 100 fs, the repetition rate is 1 kHz, and the working wavelength is 800 nm. Depending on the fabrication depth, the writing pulse energy ranges from 100 to 200 nJ, and the scanning speed varies between 50 and 100 $\mu m \cdot s^{-1}$. The fabrication precision is determined by the size of the focal spot inside the crystal, which is approximately 1.2 and 5 μm in the transverse and axial directions, respectively. Note that the laser-writing parameters (pulse energy, velocity, etc.) for $\chi^{(2)}$ erasure are critically dependent on the characteristics of the crystals, varying significantly among, e.g., the congruent, MgO-doped, and stoichiometric $LiNbO_3$ crystals.

This laser $\chi^{(2)}$-erasing technique can be traced back to two pioneering works. In 2013, Thomas *et al*. [38] used femtosecond laser pulses to reduce the nonlinear coefficients of an *x*-cut $LiNbO_3$ crystal and produced both 1D and 2D QPM structures. In 2015, Kroesen *et al*. successfully fabricated an NPC waveguide with periodically laser-erased $\chi^{(2)}$ in a *z*-cut $LiNbO_3$ crystal [39]. Recently, the same technique was also extended to the fabrication of surface $\chi^{(2)}$ structure on a birefringence phase-matching crystal, which was utilized for high-efficiency nonlinear beam shaping [40] and nonlinear holography [41]. In these works, the nonlinear crystal was cut at a specific angle to fulfill the birefringence phase-matching condition, while the amplitude-modulated $\chi^{(2)}$ structure was laser-written on the crystal surface to satisfy the transverse Raman–Nath-type phase matching.

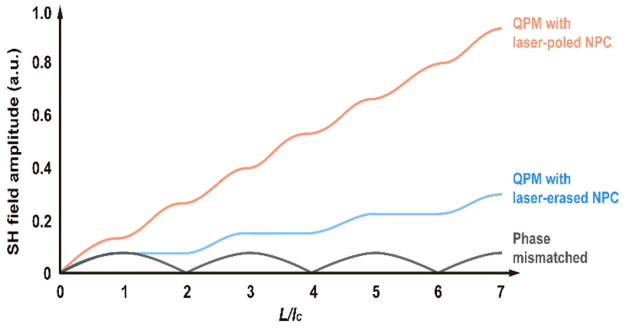

Fig. 4. Dependences of SH field on various phase-matching configurations.

The unique advantages of the laser-erased fabrication of 3D NPCs can be summarized in three main points. First, the experimental requirements for the laser-erasing technique are relatively easy to satisfy. In principle, the method requires the laser pulse energy to be above the damage threshold of the nonlinear crystal. Second, this technique provides a feasible way to fabricate 1D, 2D, and 3D NPC structures in the most commonly used nonlinear crystals at arbitrary locations and geometric orientations. Considering that it is still difficult to realize 3D domain inversion inside many single-crystal nonlinear materials, this technique could be particularly useful for $LiNbO_3$, BBO, and KTP crystals. In addition, the $\chi^{(2)}$-erasing approach can be used to engineer nonlinear optical response in materials other than ferroelectrics. For instance, the generation of higher harmonics in the ultraviolet in laser-processed quartz has been demonstrated recently [42].

In the NPCs formed via laser $\chi^{(2)}$ erasure in a $LiNbO_3$ crystal, the amplitude of the second-order nonlinear coefficient varies periodically, but its sign remains the same. Therefore, the QPM interactions are obtained via its amplitude modulation, rather than the phase modulation in the periodically poled $LiNbO_3$ crystals. Considering an ideal periodic $\chi^{(2)}$ reduction, i.e., $\chi^{(2)}$ is completely erased in the laser-exposed areas, the SH field increases over the first coherent length, remains unchanged over the second one, and then its energy increases again. Although it is less efficient than that in a traditional periodically poled nonlinear crystal, the conversion efficiency in such an $\chi^{(2)}$-erased $LiNbO_3$ crystal is still significantly enhanced in comparison to the nonphase-matching cases. For a quantitative comparison, the calculated second-harmonic intensities versus the interaction distance are presented in Fig. 4 for the $\chi^{(2)}$ erasure and $\chi^{(2)}$ inversion schemes, respectively.

B. Laser-Induced Ferroelectric Domain Inversion

The femtosecond infrared light-induced inversion of ferroelectric domains was first demonstrated in z-cut congruent $LiNbO_3$ crystal [43]. The illumination of the crystal with tightly focused infrared pulses at 800 nm (Coherent Mira, repetition rate of 76 MHz, pulse duration 180 fs) led to the appearance of inverted domains in the focus area of the laser beam. Pushing the focus down along the crystal's depth direction facilitated formation of long domains, extending from the surface up to 100 μm deep in the $LiNbO_3$ crystal [Fig. 3(b)]. This is advantageous, since the earlier optical poling with UV light produced very thin and shallow domains (usually 1–2 μm starting from the surface) because of the strong UV absorption [44]. The quality of the near-infrared laser-induced domain inversion was also confirmed by producing a 10 mm long QPM structure (with a period of 2.45 μm) to generate the SH wave with a measured conversion efficiency of 17.5% [45]. The short pulse domain inversion does not introduce any additional propagation losses for both fundamental and SH waves. The measured average loss caused by the laser-inscribed periodic domain structures in the congruent $LiNbO_3$ crystal was below 0.06 dB/cm [45].

The near-infrared short pulse poling enables 3D ferroelectric domain patterning in the bulk of ferroelectric crystals. In 2018, a simple tetragonal ferroelectric domain structure with a period of $15 \times 15 \times 64$ μm was realized in an x-cut barium calcium titanate (BCT, $Ba_{0.77}Ca_{0.23}TiO_3$) crystal [31] [Fig. 3(c)]. Compared with the $LiNbO_3$ crystal, the BCT has a much lower coercive field, so it is easier to form localized inverted domains in this crystal. Even though the first example of 3D domain structures contained only several QPM periods, it has enabled efficient control of the Čerenkov SH emission (both angle and strength) based on its unique distribution of reciprocal lattice vectors in 3D configuration. Very recently, 3D multilayer domain structures have been fabricated in the z-cut $Ca_{0.28}Ba_{0.72}Nb_2O_6$ (CBN) crystals [46]. Figure 3(d) shows an example of the three-layer structure containing fork, linear grating, and circular grating, domain patterns designed for nonlinear wavefront shaping. The transverse period of these structures is 2 μm, which can be further improved to reach submicrometer scale by optimizing the laser-writing conditions.

The near-infrared short pulse poling method relies on nonlinear absorption of light in the optical beam's focal volume, which, in turn, induces a high temperature gradient and the appearance of a thermoelectric field to locally invert the direction of the spontaneous polarization [31,43,47,48]. This physical process is very similar to the UV light poling, except that the nonlinear instead of linear absorption is employed in the former case. The light-induced thermoelectric field is a simplified and straightforward model that can explain the most experimental observations, but it needs further improvement to clarify all the puzzles. In fact, the ferroelectric domain inversion formed by high-intensity infrared laser pulses is a complex physical process involving, in addition to formation of thermoelectric field, many other factors, such as pyroelectric effect, bulk screening, and the presence of free charges. Also, differences between ferroelectric crystals may also play a role. Complete understanding of the all-optically induced ferroelectric domain inversion process does certainly require further investigations.

C. Differences in Experimental Conditions between the Laser-Induced $\chi^{(2)}$ Erasure and $\chi^{(2)}$ Inversion Approaches

The laser-induced $\chi^{(2)}$ erasure and $\chi^{(2)}$ inversion approaches are based on two different physical mechanisms, i.e., crystallinity reduction and light-induced electric field poling, respectively, which decide that the fabrication strategies are quite different. For example, the laser $\chi^{(2)}$ erasing approach typically uses higher pulse energies and lower repetition rates as compared to the laser $\chi^{(2)}$ inversion method. In comparison to a $\chi^{(2)}$-erased NPC, the $\chi^{(2)}$ modulation depth in a $\chi^{(2)}$-reversed NPC is doubled, and the conversion efficiency is quadrupled correspondingly. Notably, the laser $\chi^{(2)}$ erasing approach can be applicable to materials other than typical ferroelectric crystals. The differences in laser writing conditions between these two methods are summarized in Table 1.

3. CHARACTERIZATIONS OF 3D NPCs

The traditional chemical selective etching method works well to visualize ferroelectric domain structures at or close to surfaces, but it is less useful when 3D structure visualization is required. While part of the crystal can be removed to access the target domain structure, this method is destructive. So far, the Čerenkov SH microscopy [49] and the QPM-based approach have been used in diagnostic of 3D structures fabricated by both methods discussed above [30,31,36,46]. As an essential complement, piezoresponse force microscopy (PFM) is used for confirming the ferroelectric domain inversion [50,51], and the micro-Raman scattering and transmission electron microscope (TEM) are used for analysis of $\chi^{(2)}$ reduction [30].

A. Čerenkov SH Microscopy

The Čerenkov SH microscopy is a straightforward way to visualize the spatial $\chi^{(2)}$ variation inside a nonlinear crystal. The Čerenkov SH signal is emitted along a specific angle defined by the longitudinal phase-matching condition, and it gets much stronger in the region of sharp $\chi^{(2)}$ modulation, i.e., at the interface between different $\chi^{(2)}$ signs (ferroelectric domain wall) or $\chi^{(2)}$ amplitudes [52,53]. 3D visualization of nonlinear photonic structures is obtained by scanning a tightly focused fundamental beam across the sample and recording the corresponding Čerenkov SH signal at each position [49]. Čerenkov microscopy is a nondestructive imaging method, producing high-contrast images and offering an exceptional spatial resolution as a result of the second-order nonlinear process (see Fig. 3).

Čerenkov SH microscopy provides an important tool to visualize domain structures created by the electric-field poling. However, it may not be sufficient to fully determine the physical properties of the laser-induced structures. The point is that both domain inversion and $\chi^{(2)}$ erasure can lead to Čerenkov harmonic emission. Besides, the intense light pulses can also lead to other effects such as refractive index variation of the crystal. To clarify these issues, PFM is generally used in the scheme of domain inversion. PFM is a variant of atomic force microscopy (AFM), which provides a direct way to determine the orientation of ferroelectric domains [50,51]. It works on the converse piezoelectric effect of ferroelectric crystals, i.e., with an applied electric field, the ferroelectric domains will expand or shrink depending on the polarity of the former. A typical PFM image of the ferroelectric domain structure created by femtosecond laser writing is shown in Fig. 5(a).

To characterize the 3D NPC fabricated using laser erasure of $\chi^{(2)}$, micro-Raman scattering and TEM are used as two standard methods for analyzing the crystallinity of the crystal. The intensity of the Raman peak is a function of the polarizability of the molecule excited by an external field. As shown in Fig. 5(b), the Raman resonance peaks in the laser-erased area are significantly suppressed in comparison to the original ones. This indicates a strong restriction on the vibrational degrees of freedom of the molecule, which can be attributed to the reduced crystallinity in the fabricated area, also an indication of $\chi^{(2)}$ reduction. The TEM diffraction works in a similar way. It shows sharp diffraction peaks in the nonprocessed area, but the peaks become vague when moving to the processed area [see Fig. 5(c)]. In principle, for an ideal structure with a completely erased $\chi^{(2)}$, both Raman peaks and TEM diffractions will disappear in the laser-processed areas.

It is worth noting that the $\chi^{(2)}$-erased structure can also be visualized by the common SH microscopy owing to the reduced amplitude of $\chi^{(2)}$ in the laser-written areas [30]. However, Čerenkov SH microscopy offers much better signal-to-noise ratio, resolution, and sensitivity because the longitudinal phase-matched nonlinear Čerenkov signal is much stronger than the

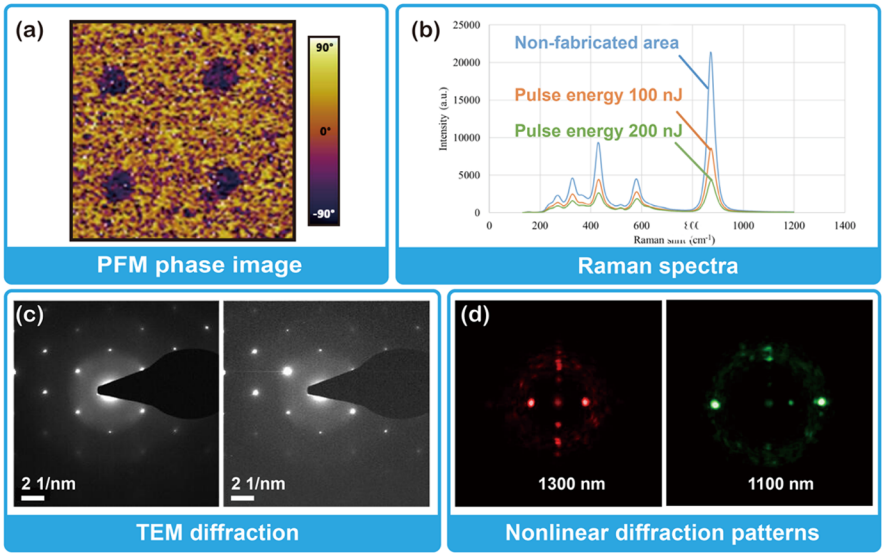

Fig. 5. Characterization approaches for the 3D NPCs. (a) Typical PFM image of laser-engineered ferroelectric domain structure in a $Ca_{0.28}Ba_{0.72}Nb_2O_6$ (CBN) crystal; the optically inverted domains distribute as a square lattice. The random orientation of ferroelectric domains in the surroundings correspond to the naturally random domain structure of the host CBN crystal. (b) The micro-Raman scattering and (c) TEM to analyze the $\chi^{(2)}$-reduced structures. The Raman peaks get weaker, and the TEM diffraction pattern turns vague with the reduction of $\chi^{(2)}$ amplitude. (d) The variation of nonlinear diffraction pattern from a multiplayer 3D NPC with the fundamental wavelength [46]. The first-order nonlinear Raman–Nath diffraction (in the horizontal direction) is the strongest at a fundamental wavelength of 1300 nm, but the second-order diffraction becomes much stronger at 1100 nm (because the second-order diffraction coincides with the Čerenkov SH angle now). The variation of the relative strength of diffraction orders with wavelength is a unique feature of nonlinear interaction caused by periodic $\chi^{(2)}$ modulation. The figure is reprinted with permission from [30].

forward mismatched harmonic beam that is used in the latter case [54].

B. QPM-Based Characterization Approaches

The observation of QPM-related nonlinear optical effects is an alternative type of approach for confirming the $\chi^{(2)}$ modulation induced by the laser pulses. These nonlinear optical effects occur because of the periodic modulation of $\chi^{(2)}$, so they can be used to characterize both $\chi^{(2)}$-reversed and $\chi^{(2)}$-reduced 3D structures. A difference is that the conversion efficiency of these nonlinear effects are usually higher in the $\chi^{(2)}$-reversed scheme where the Fourier coefficient is stronger [Fig. 4]. One straightforward way is to produce a periodic QPM structure and check if the SH signal is stronger than that from the nonengineered areas. This process usually involves fabrication of a long structure with many periods, which is time-consuming for the laser-writing procedure. It is known that the nonlinear frequency conversions can also occur with fulfillment of only transverse or longitudinal phase matching conditions, which are called nonlinear Raman–Nath diffraction [22] and nonlinear Čerenkov radiation [52], respectively. Therefore, more convenient ways are available by observing the influence of these two kinds of nonlinear emissions by the laser-induced 3D patterns.

One possibility is to observe the variation of the nonlinear Raman–Nath diffraction pattern with the fundamental wavelength. In this case, the fundamental beam propagates perpendicularly to the $\chi^{(2)}$ modulation, and the diffracted SH wave can be obtained in a way similar to the linear diffraction from a refractive-index grating. If the SH diffraction is indeed caused by the $\chi^{(2)}$ modulation, the strongest diffraction will appear at higher orders coinciding with the Čerenkov SH angle [Fig. 5(d)]. On the contrary, the relative strength of different diffraction orders is independent of the wavelength if it is a linear optical process, i.e., caused by the periodic variation of refractive index of the crystal.

The other way is to compare the nonlinear Čerenkov radiation from laser-engineered and nonengineered areas. Note that here the Čerenkov SH is generated with a loosely focused fundamental beam covering many $\chi^{(2)}$ periods, while in Čerenkov second-harmonic microscopy, the fundamental beam is tightly focused to cover a single domain wall. Due to the $\chi^{(2)}$ periodicity, the intensity of the Čerenkov second-harmonic signal is sensitive to the fundamental wavelength, i.e., it shows resonant peaks with the wavelength tuning [55,56]. Moreover, being dependent on the participation of reciprocal lattice vectors along the propagation directions of fundamental beam, the Čerenkov SH may be emitted at bigger/smaller angles, determined by $k_2 \cos\theta = 2k_1 + G_h$, with G_h being the reciprocal lattice vector in the propagation direction of the fundamental beam [31].

4. APPLICATIONS OF LASER-ENGINEERED NPCs

A. QPM Structures for Efficient Frequency Conversion in Atypical Interaction Geometries

The laser engineering of nonlinear coefficient $\chi^{(2)}$ offers a number of exciting applications. The primary and most obvious application is to provide an alternative route to standard electrical poling in fabrication of QPM structures, as the latter is a rather cumbersome process combining few complex steps such as lithography for electrodes patterning and high-voltage application for the domain reversal. The laser-writing approach can deliver the same outcome in just one step. The $\chi^{(2)}$ modulation can be conducted at any stage of nonlinear circuit fabrication, as long as the area of interest is accessible for the laser beam. Furthermore, the laser-writing approach allows one to create nonlinear structures in thick samples where standard electrical poling is not possible due to the high value of the coercive field, such as in $LiNbO_3$, where >20 kV/mm coercive field restricts practical material thickness to hundreds of micrometers. In particular, it has been shown that laser-induced local damage in the ferroelectric crystals may stimulate inception and growth of inverted domains up to the opposite surfaces of the crystal, allowing for the formation of $\chi^{(2)}$ patterns [57]. Moreover, multiple QPM structures of various complexity and periods could be imprinted at will in different locations of the same crystal [46], a feature that is hard to achieve with the standard electrical poling technique. It also enables one to create spatially confined nonlinear structures at different depths of the same sample inside already existing refractive index structures such as waveguides. For instance, various nonlinear gratings were imprinted in laser-written waveguides in $LiNbO_3$ crystal [37]. In addition, the laser-beam-writing approach can be employed in nonstandard geometries where the use of electrical poling is either extremely difficult or virtually impossible, such as in x-cut crystals [31].

B. 3D NPCs for Simultaneous Wave Interaction and Nonlinear Data Processing

The significance of laser-based $\chi^{(2)}$ modulation lies in its ability to arbitrarily modulate the nonlinearity in almost any locations inside the ferroelectrics. In this way, one can create 3D $\chi^{(2)}$ structures of various symmetries. Such 3D nonlinearity patterns can be employed for realization of nonlinear parametric interactions in many directions, taking advantage of spatially dependent periodicity and strength. The basic proof-of-principle demonstrations have already been carried out by creating the first 3D NPCs in BTC and $LiNbO_3$ crystals [30,31]. These simple structures of rectangular symmetry have enabled fulfilment of phase-matching conditions of nonlinear optical interactions along various spatial directions [Fig. 6(a)] and offered unique flexibility to control optical emissions at new frequencies, such as to steer the nonlinear Čerenkov radiation to any spatial direction [Fig. 6(b)]. The advantage of utilizing 3D structures was further confirmed by creating multilayer $\chi^{(2)}$ patterns overlapping in transverse dimension but located at different depths in the medium for dynamical control of the SH emissions by tuning the focus location inside the crystal [Fig. 6(c)] [46].

C. Applications in Nonlinear Beam Shaping: Generation of Structured Light Beams and Nonlinear Volume Holograms

Spatial nonlinear structures involving 3D complex patterns can be also used for the nonlinear wave shaping, when the nonlinear interactions lead to generation of new frequencies (e.g., SHs) with predesigned intensity and phase profiles. Multiple optical vortices and higher-order Hermite–Gaussian beams have been generated in simple laser-induced structures [30,40,46,58]. With improved resolution and minimized scattering losses, the technique allows one to create nonlinear volume holograms for efficient frequency conversion combined with wavefront shaping for potential applications in optical processing, quantum entanglement, etc.

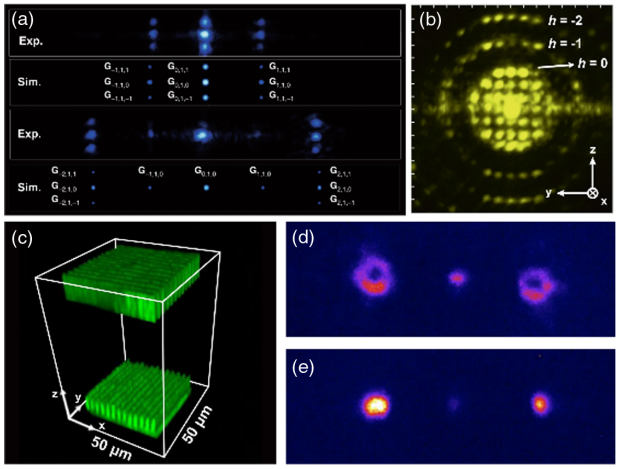

Fig. 6. (a) Simultaneous SHG along different directions in a $LiNbO_3$ NPC. The figure is reprinted with permission from [30]. (b) The generation of multiple Čerenkov SH rings in a 3D BCT NPC. The strengths and emission angles of these rings are adjustable thanks to the 3D $\chi^{(2)}$ modulation. The figure is reprinted with permission from [31]. (c) A two-layer CBN crystal for dynamical generation of SH waves. When the focus of the fundamental beam moves from the top ($\chi^{(2)}$ fork structure) to bottom ($\chi^{(2)}$ grating) domain pattern, the generated SH waves change from (d) vortex beams (e) into Gaussian beams. The figures are reprinted with permission from [46].

The nonlinear volume holography works analogously to its linear counterpart, but it enables reconstruction of object wave at a frequency different from the input one as a consequence of $\chi^{(2)}$ modulation. It has a form of interference pattern between the polarization wave with twice the fundamental frequency 2ω and the SH wave with a predesigned wavefront, which is then binarized and recorded as $\chi^{(2)}$ modulations in a nonlinear crystal. Due to the lack of techniques that are capable of 3D $\chi^{(2)}$ engineering, most of the previous studies of nonlinear holography were restricted to 2D structures with a rather low efficiency. In fact, these 2D schemes represent thin rather than volume holograms. While the principle of nonlinear volume holography was demonstrated in 2014 [59], the real nonlinear volume holograms were realized only after the discovery of 3D $\chi^{(2)}$ engineering with near-infrared femtosecond laser pulses [60]. The design, fabrication, and nonlinear reconstruction of a 3D nonlinear volume hologram for a SH vortex beam are shown in Fig. 7 as an example. In principle, the nonlinear volume holography in 3D NPCs provides a universal approach for efficient generation of structured light beams at new frequencies.

D. 3D Ferroelectric Domain Structures for Synthesis of Gauge Fields

It has been shown recently that the equations governing nonlinear parametric interaction are mathematically equivalent to quantum mechanical formalism, describing the dynamics of spin particles in spatially varying magnetic fields [61–63]. These gauge fields are represented by spatially complex nonlinearity patterns. Because of electrical poling restrictions, only simple processes have been experimentally realized so far. Employing the potential for making arbitrary patterns with 3D laser-induced $\chi^{(2)}$ modulation offers an unique opportunity to create nonlinear structures that could mimic 3D complex magnetic and electric fields for realization of optical analogs of subtle quantum mechanical phenomena.

5. CONCLUSION AND OUTLOOK

3D NPCs appear to be indispensable in nonlinear optics and advanced photonics to control nonlinear interacting waves in entire space. In experiment, 3D NPCs with tetragonal, periodic fork, and multilayer structures have been tested in SHG processes, in which the generated multiple SH signals well confirm the 3D QPM theory. It is expected to accomplish more advanced tasks including high-density data security storage and nonlinear multiplexing holography, demanding precise fabrication of more complicated 3D $\chi^{(2)}$-modulated structures such as the quasi-crystal structure and chirped pattern. In addition, so far only the simplest SHG process has been demonstrated in 3D NPCs. With one more pump wavelength, one can realize sum-frequency generation, difference-frequency generation, and even terahertz generation with predesigned beam profiles. Also, 3D NPC is capable of mediating optical parametric downconversion, including optical parametric oscillator (OPO) and optical parametric amplifier (OPA) processes, which can be further extended to quantum optics, as will be discussed below. The cascaded $\chi^{(2)}$ effect is another interesting direction, considering that 3D NPCs can provide abundant channels for nonlinear cascading in 3D space.

1D and 2D NPCs have been proven to be important and efficient in producing quantum entanglements in energy-time, polarization, spatial mode, and path. The experimental realization

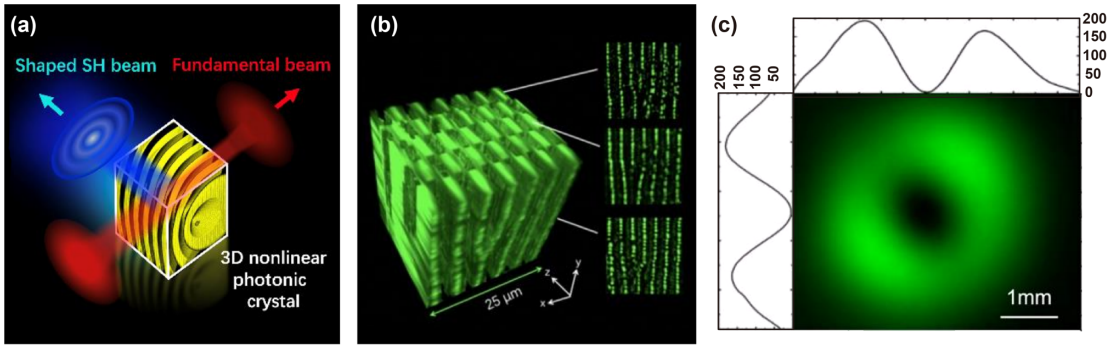

Fig. 7. (a) Illustrating the concept of nonlinear volume holography. The interference pattern between the nonlinear polarization wave at frequency 2ω (reference beam) and the SH wave with a predesigned wavefront (objective beam) is recorded as a binary $\chi^{(2)}$ modulation pattern inside the 3D NPC. When such a crystal is illuminated by the fundamental wave, reconstruction of the SH beam is obtained. (b) An experimental example of nonlinear volume holograms created by interfering a polarization Gaussian wave and the SH vortex beam in a CBN crystal; (c) experimentally recorded far-field image of the SH vortex generated from the nonlinear volume hologram in (b); the figures are reprinted with permission from [60].

of 3D NPCs can push these applications in quantum optics and quantum technologies to a higher level. Since the full QPM conditions and wavefront modulation can be simultaneously achieved, it should be possible to realize high-dimensional entanglements in 3D NPC devices. For example, entanglement of orbital angular momentum (OAM) states was typically realized by adding a spatial light modulator to sort the OAM states [64]. Now, the same functionality can be readily realized in a periodic 3D $\chi^{(2)}$ fork-type grating. Recently, a 100-path photon–pair source was reported in a hybrid device of a metalens array and BPM crystal [65]. 3D NPC offers the opportunity to integrate these functions into a single crystal. In addition, as the femtosecond laser fabrication method for 3D NPCs is fully compatible with the existing optical fabrication techniques, including the ultrafast laser writing of waveguides, microdisks, and other complex micro/nano refractive indices, one can easily combine the newly developed 3D QPM structures and 3D waveguide arrays to achieve powerful integrated 3D photonic devices for quantum information processing and quantum communications.

The optical poling method used for the fabrication of 3D NPCs may also pave the way to achieve high-performance ferroelectric-domain wall-based devices. The recent discoveries of giant photovoltaic effect and electrical conductivity in some types of ferroelectric domain walls have enabled domain-wall-based photovoltaic devices and nonvolatile memories [66]. The performance of these devices is critically dependent on distributions and shapes of ferroelectric domain walls, whose control by traditional electric-field poling is complex and inflexible. The femtosecond laser poling platform offers an ideal technique to construct such domain-wall-based devices, enabling localized precise control of ferroelectric domains and, more significantly, the creation of 3D domain walls to boost the photovoltaic and microelectronic performances.

Besides optics, the study of nonlinear wave interactions in 3D configuration may inspire exploration of similar phenomena in other systems, including, for instance, the generation and control of acoustic waves in dielectrics and matter waves in optical lattices. In particular, it has been shown that the periodically poled $LiNbO_3$ can act as an excellent phononic crystal for acoustic wave control with an applied low-voltage electric field [67]. With the femtosecond laser $\chi^{(2)}$ engineering techniques, the concept of 2D $LiNbO_3$ phononic crystals can be naturally extended to 3D configurations, enabling more efficient controls of acoustic waves with complete bandgap structures in three full dimensions.

The major technical challenge is to fabricate efficiently high-precision large-scale 3D NPCs. The typical dimensions of 3D NPCs reported in recent experiments do not exceed a hundred micrometers. A significant size expansion to several millimeters (especially in the light propagation direction) is necessary to improve the conversion efficiency for many practical applications. Multifocal laser-writing systems could be employed as an effective way to facilitate fast fabrication of 3D NPCs on a large scale. Another challenging issue is to achieve highly precise $\chi^{(2)}$ engineering in 3D, which is mainly limited by the focal spot size of the writing laser beam. Especially along the depth direction of the crystal, the laser focus is prone to deformation and even splitting due to spherical aberrations and birefringence, further lowering the longitudinal resolution. To solve the issue, one may apply a few countermeasures, such as selecting the proper polarization state of the laser beam and preshaping the beam's wavefront using a spatial light modulator to achieve a submicrometer focus spot. When the resolution of $\chi^{(2)}$ engineering is reduced down to submicrometer scale, 3D NPC can be applied in ultranarrow bandwidth quantum light source, high-frequency acoustic wave generation, and high-density data storage.

Funding. National Key Research and Development Program of China (2016YFA0302500, 2017YFA0303703); National Natural Science Foundation of China (11874213, 91950206); Australian Research Council (DP19010774); Qatar National Research Fund (NPRP 12S-0205-190047).

Acknowledgment. The authors thank Tianxin Wang and Shan Liu for their comments and support in preparation of Figs. 1 and 5.

Disclosures. The authors declare no competing interests.

REFERENCES

1. P. A. Franken, A. E. Hill, C. W. Peters, and G. Weinreich, "Generation of optical harmonics," Phys. Rev. Lett. **7**, 118–119 (1961).
2. N. Mazumder, N. K. Balla, G.-Y. Zhuo, Y. V. Kistenev, R. Kumar, F.-J. Kao, S. Brasselet, V. V. Nikolaev, and N. A. Krivova, "Label-free nonlinear multimodal optical microscopy—basics, development, and applications," Front. Phys. **7**, 170 (2019).
3. L. Chang, A. Boes, H. Shu, W. Xie, H. Huang, J. Qin, B. Shen, X. Wang, A. Mitchell, and J. E. Bowers, "Second order nonlinear photonic integrated platforms for optical signal processing," IEEE J. Sel. Top. Quantum Electron. **27**, 1–11 (2021).
4. D. E. Chang, V. Vuletić, and M. D. Lukin, "Quantum nonlinear optics—photon by photon," Nat. Photonics **8**, 685–694 (2014).
5. P. Ferraro, S. Grilli, and P. Natale, *Ferroelectric Crystals for Photonic Applications*, 2nd ed. (Springer, 2014).
6. P. S. Kuo, J. Bravo-Abad, and G. S. Solomon, "Second-harmonic generation using $\bar{4}$-quasi-phasematching in a GaAs whispering-gallery-mode microcavity," Nat. Commun. **5**, 3109 (2014).
7. P. Karpinski, X. Chen, V. Shvedov, C. Hnatovsky, A. Grisard, E. Lallier, B. Luther-Davies, W. Krolikowski, and Y. Sheng, "Nonlinear diffraction in orientation-patterned semiconductors," Opt. Express **23**, 14903–14912 (2015).
8. H. Nasu, H. Okamoto, K. Kurachi, J. Matsuoka, K. Kamiya, A. Mito, and H. Hosono, "Second-harmonic generation from electrically poled SiO_2 glasses: effects of OH concentration, defects, and poling conditions," J. Opt. Soc. Am. B **12**, 644–649 (1995).
9. J. A. Armstrong, N. Bloembergen, J. Ducuing, and P. S. Pershan, "Interactions between light waves in a nonlinear dielectric," Phys. Rev. **127**, 1918–1939 (1962).
10. G. A. Magel, M. M. Fejer, and R. L. Byer, "Quasi-phase-matched second-harmonic generation of blue light in periodically poled $LiNbO_3$," Appl. Phys. Lett. **56**, 108–110 (1990).
11. M. Yamada, N. Nada, M. Saitoh, and K. Watanabe, "First-order quasi-phase matched $LiNbO_3$ waveguide periodically poled by applying an external field for efficient blue second-harmonic generation," Appl. Phys. Lett. **62**, 435–436 (1993).
12. D. Feng, N. B. Ming, J. F. Hong, Y. S. Yang, J. S. Zhu, Z. Yang, and Y. N. Wang, "Enhancement of second-harmonic generation in $LiNbO_3$ crystals with periodic laminar ferroelectric domains," Appl. Phys. Lett. **37**, 607–609 (1980).
13. V. Berger, "Nonlinear photonic crystals," Phys. Rev. Lett. **81**, 4136–4139 (1998).
14. S. John, "Strong localization of photons in certain disordered dielectric superlattices," Phys. Rev. Lett. **58**, 2486–2489 (1987).
15. E. Yablonovitch, "Inhibited spontaneous emission in solid-state physics and electronics," Phys. Rev. Lett. **58**, 2059–2062 (1987).
16. N. G. R. Broderick, G. W. Ross, H. L. Offerhaus, D. J. Richardson, and D. C. Hanna, "Hexagonally poled lithium niobate: a two-dimensional nonlinear photonic crystal," Phys. Rev. Lett. **84**, 4345–4348 (2000).
17. A. Arie and N. Voloch, "Periodic, quasi-periodic, and random quadratic nonlinear photonic crystals," Laser Photon. Rev. **4**, 355–373 (2010).
18. Y. Zhang, Z. D. Gao, Z. Qi, S. N. Zhu, and N. B. Ming, "Nonlinear Čerenkov radiation in nonlinear photonic crystal waveguides," Phys. Rev. Lett. **100**, 163904 (2008).

19. K. Gallo, M. Levenius, F. Laurell, and V. Pasiskevicius, "Twin-beam optical parametric generation in $\chi^{(2)}$ nonlinear photonic crystals," Appl. Phys. Lett. **98**, 161113 (2011).
20. J. R. Kurz, A. M. Schober, D. S. Hum, A. J. Saltzman, and M. M. Fejer, "Nonlinear physical optics with transversely patterned quasi-phase-matching gratings," IEEE J. Sel. Top. Quantum Electron. **8**, 660–664 (2002).
21. P. Xu, S. H. Ji, S. N. Zhu, X. Q. Yu, J. Sun, H. T. Wang, J. L. He, Y. Y. Zhu, and N. B. Ming, "Conical second harmonic generation in a two-dimensional photonic crystal: a hexagonally poled $LiNbO_3$ crystal," Phys. Rev. Lett. **93**, 133904 (2004).
22. S. M. Saltiel, D. N. Neshev, R. Fischer, W. Krolikowski, A. Arie, and Y. S. Kivshar, "Generation of second-harmonic conical waves via nonlinear Bragg diffraction," Phys. Rev. Lett. **100**, 103902 (2008).
23. T. Ellenbogen, N. Voloch-Bloch, A. Ganany-Padowicz, and A. Arie, "Nonlinear generation and manipulation of Airy beams," Nat. Photonics **3**, 395–398 (2009).
24. N. V. Bloch, K. Shemer, A. Shapira, R. Shiloh, I. Juwiler, and A. Arie, "Twisting light by nonlinear photonic crystals," Phys. Rev. Lett. **108**, 233902 (2012).
25. H. Y. Leng, X. Q. Yu, Y. X. Gong, P. Xu, Z. D. Xie, H. Jin, C. Zhang, and S. N. Zhu, "On-chip steering of entangled photons in nonlinear photonic crystals," Nat. Commun. **2**, 429 (2011).
26. S. Trajtenberg-Mills, A. Karnieli, N. Voloch-Bloch, E. Megidish, H. S. Eisenberg, and A. Arie, "Simulating correlations of structured spontaneously down-converted photon pairs," Laser Photon. Rev. **14**, 1900321 (2020).
27. J. Chen and X. Chen, "Phase matching in three-dimensional nonlinear photonic crystals," Phys. Rev. A **80**, 013801 (2009).
28. J. Chen and X. Chen, "Generation of conical and spherical second harmonics in three-dimensional nonlinear photonic crystals with radial symmetry," J. Opt. Soc. Am. B **28**, 241–246 (2011).
29. T. Pogosian and N. D. Lai, "Theoretical investigation of three-dimensional quasi-phase-matching photonic structures," Phys. Rev. A **94**, 063821 (2016).
30. D. Wei, C. Wang, H. Wang, X. Hu, D. Wei, X. Fang, Y. Zhang, D. Wu, Y. Hu, J. Li, S. Zhu, and M. Xiao, "Experimental demonstration of a three-dimensional lithium niobate nonlinear photonic crystal," Nat. Photonics **12**, 596–600 (2018).
31. T. Xu, K. Switkowski, X. Chen, S. Liu, K. Koynov, H. Yu, H. Zhang, J. Wang, Y. Sheng, and W. Krolikowski, "Three-dimensional nonlinear photonic crystal in ferroelectric barium calcium titanate," Nat. Photonics **12**, 591–595 (2018).
32. S. Keren-Zur and T. Ellenbogen, "A new dimension for nonlinear photonic crystals," Nat. Photonics **12**, 575–577 (2018).
33. R. R. Gattass and E. Mazur, "Femtosecond laser micromachining in transparent materials," Nat. Photonics **2**, 219–225 (2008).
34. K. Sugioka and Y. Cheng, "Femtosecond laser three-dimensional micro- and nanofabrication," Appl. Phys. Rev. **1**, 041303 (2014).
35. M. Malinauskas, A. Žukauskas, S. Hasegawa, Y. Hayasaki, V. Mizeikis, R. Buividas, and S. Juodkazis, "Ultrafast laser processing of materials: from science to industry," Light Sci. Appl. **5**, e16133 (2016).
36. D. Wei, C. Wang, X. Xu, H. Wang, Y. Hu, P. Chen, J. Li, Y. Zhu, C. Xin, X. Hu, Y. Zhang, D. Wu, J. Chu, S. Zhu, and M. Xiao, "Efficient nonlinear beam shaping in three-dimensional lithium niobate nonlinear photonic crystals," Nat. Commun. **10**, 4193 (2019).
37. J. Imbrock, L. Wesemann, S. Kroesen, M. Ayoub, and C. Denz, "Waveguide-integrated three-dimensional quasi-phase-matching structures," Optica **7**, 28–34 (2020).
38. J. Thomas, V. Hilbert, R. Geiss, T. Pertsch, A. Tünnermann, and S. Nolte, "Quasi phase matching in femtosecond pulse volume structured x-cut lithium niobate," Laser Photon. Rev. **7**, L17–L20 (2013).
39. S. Kroesen, K. Tekce, J. Imbrock, and C. Denz, "Monolithic fabrication of quasi phase-matched waveguides by femtosecond laser structuring the $\chi^{(2)}$ nonlinearity," Appl. Phys. Lett. **107**, 101109 (2015).
40. B. Zhu, H. Liu, Y. Chen, and X. Chen, "High conversion efficiency second-harmonic beam shaping via amplitude-type nonlinear photonic crystals," Opt. Lett. **45**, 220–223 (2019).
41. B. Zhu, H. Liu, Y. Liu, X. Yan, Y. Chen, and X. Chen, "Second-harmonic computer-generated holographic imaging through monolithic lithium niobate crystal by femtosecond laser micromachining," Opt. Lett. **45**, 4132–4135 (2020).
42. M. Shao, F. Liang, H. Yu, and H. Zhang, "Pushing periodic-disorder-induced phase matching into the deep-ultraviolet spectral region: theory and demonstration," Light Sci. Appl. **9**, 45 (2020).
43. X. Chen, P. Karpinski, V. Shvedov, K. Koynov, B. X. Wang, J. Trull, C. Cojocaru, W. Krolikowski, and Y. Sheng, "Ferroelectric domain engineering by focused infrared femtosecond pulses," Appl. Phys. Lett. **107**, 141102 (2015).
44. C. Y. J. Ying, A. C. Muir, C. E. Valdivia, H. Steigerwald, C. L. Sones, R. W. Eason, E. Soergel, and S. Mailis, "Light-mediated ferroelectric domain engineering and micro-structuring of lithium niobate crystals," Laser Photon. Rev. **6**, 526–548 (2012).
45. X. Chen, P. Karpinski, V. Shvedov, A. Boes, A. Mitchell, W. Krolikowski, and Y. Sheng, "Quasi-phase matching via femtosecond laser-induced domain inversion in lithium niobate waveguides," Opt. Lett. **41**, 2410–2413 (2016).
46. S. Liu, K. Switkowski, C. Xu, J. Tian, B. Wang, P. Lu, W. Krolikowski, and Y. Sheng, "Nonlinear wavefront shaping with optically induced three-dimensional nonlinear photonic crystals," Nat. Commun. **10**, 3208 (2019).
47. H. Zhu, X. Chen, H. Chen, and X. Deng, "Formation of domain reversal by direct irradiation with femtosecond laser in lithium niobate," Chin. Opt. Lett. **7**, 169–172 (2009).
48. H. Lao, H. Zhu, and X. Chen, "Threshold fluence for domain reversal directly induced by femtosecond laser in lithium niobate," Appl. Phys. A **101**, 313–317 (2010).
49. Y. Sheng, A. Best, H. J. Butt, W. Krolikowski, A. Arie, and K. Koynov, "Three-dimensional ferroelectric domain visualization by Čerenkov-type second harmonic generation," Opt. Express **18**, 16539–16545 (2010).
50. A. Gruverman and S. V. Kalinin, "Piezoresponse force microscopy and recent advances in nanoscale studies of ferroelectrics," J. Mater. Sci. **41**, 107–116 (2006).
51. E. Soergel, "Piezoresponse force microscopy (PFM)," J. Phys. D **44**, 464003 (2011).
52. S. M. Saltiel, Y. Sheng, N. Voloch-Bloch, D. N. Neshev, W. Krolikowski, A. Arie, K. Koynov, and Y. S. Kivshar, "Cerenkov-type second-harmonic generation in two-dimensional nonlinear photonic structures," IEEE J. Quantum Electron. **45**, 1465–1472 (2009).
53. Y. Sheng, V. Roppo, K. Kalinowski, and W. Krolikowski, "Role of a localized modulation of $\chi^{(2)}$ in Čerenkov second-harmonic generation in nonlinear bulk medium," Opt. Lett. **37**, 3864–3866 (2012).
54. X. Huang, D. Wei, Y. Wang, Y. Zhu, Y. Zhang, X. P. Hu, S. N. Zhu, and M. Xiao, "Second-harmonic interference imaging of ferroelectric domains through a scanning microscope," J. Phys. D **50**, 485105 (2017).
55. K. Kalinowski, Q. Kong, V. Roppo, A. Arie, Y. Sheng, and W. Krolikowski, "Wavelength and position tuning of Čerenkov second-harmonic generation in optical superlattice," Appl. Phys. Lett. **99**, 181128 (2011).
56. Y. Sheng, Q. Kong, V. Roppo, K. Kalinowski, Q. Wang, C. Cojocaru, and W. Krolikowski, "Theoretical study of Čerenkov-type second-harmonic generation in periodically poled ferroelectric crystals," J. Opt. Soc. Am. B **29**, 312–318 (2012).
57. J. Imbrock, H. Hanafi, M. Ayoub, and C. Denz, "Local domain inversion in MgO-doped lithium niobate by pyroelectric field-assisted femtosecond laser lithography," Appl. Phys. Lett. **113**, 252901 (2018).
58. D. Liu, S. Liu, L. M. Mazur, B. Wang, P. Lu, W. Krolikowski, and Y. Sheng, "Smart optically induced nonlinear photonic crystals for frequency conversion and control," Appl. Phys. Lett. **116**, 051104 (2020).
59. X. H. Hong, B. Yang, C. Zhang, Y. Q. Qin, and Y. Y. Zhu, "Nonlinear volume holography for wave-front engineering," Phys. Rev. Lett. **113**, 163902 (2014).
60. S. Liu, L. M. Mazur, W. Krolikowski, and Y. Sheng, "Nonlinear volume holography in 3D nonlinear photonic crystals," Laser Photon. Rev. **14**, 2000224 (2020).
61. A. Karnieli and A. Arie, "All-optical Stern-Gerlach effect," Phys. Rev. Lett. **120**, 053901 (2018).
62. A. Karnieli, S. Trajtenberg-Mills, G. Di Domenico, and A. Arie, "Experimental observation of the geometric phase in nonlinear frequency conversion," Optica **6**, 1401–1405 (2019).
63. A. Karnieli, S. Tsesses, G. Bartal, and A. Arie, "Optical skyrmions and a topological Hall effect in artificial gauge fields," in *Conference on Lasers and Electro-Optics (CLEO)* (2020), paper FW4A.6.
64. J. Leach, B. Jack, J. Romero, A. K. Jha, A. M. Yao, S. Franke-Arnold, D. G. Ireland, R. W. Boyd, S. M. Barnett, and M. J. Padgett, "Quantum correlations in optical angle–orbital angular momentum variables," Science **329**, 662–665 (2010).

65. L. Li, Z. Liu, X. Ren, S. Wang, V.-C. Su, M.-K. Chen, C. H. Chu, H. Y. Kuo, B. Liu, W. Zang, G. Guo, L. Zhang, Z. Wang, S. Zhu, and D. P. Tsai, "Metalens-array–based high-dimensional and multiphoton quantum source," Science **368**, 1487–1490 (2020).
66. R. Guo, L. You, Y. Zhou, Z. S. Lim, X. Zou, L. Chen, R. Ramesh, and J. L. Wang, "Non-volatile memory based on the ferroelectric photovoltaic effect," Nat. Commun. **4**, 1990 (2013).
67. D. Yudistira, A. Boes, B. Djafari-Rouhani, Y. Pennec, L. Y. Yeo, A. Mitchell, and J. R. Friend, "Monolithic phononic crystals with a surface acoustic band gap from surface phonon-polariton coupling," Phys. Rev. Lett. **113**, 215503 (2014).